EUROPEAN FUSION DEVELOPMENT AGREEMENT

EFDA–JET–CP(07)03/32

L. Colas, A. Ekedahl, M. Goniche, J.P. Gunn, B. Nold, Y. Corre, V. Bobkov, R. Dux, F. Braun, J-M. Noterdaeme, M.-L. Mayoral, K. Kirov, J. Mailloux, S. Heuraux, E. Faudot, J. Ongena, ASDEX Upgrade team and JET EFDA contributors

Understanding the Spatial structure of RF-induced SOL Modifications

Understanding the Spatial structure of RF-induced SOL Modifications

L. Colas[1], A. Ekedahl[1], M. Goniche[1], J.P. Gunn[1], B. Nold[1], Y. Corre[1], V. Bobkov[2], R. Dux[2], F. Braun[2], J-M. Noterdaeme[2], M.-L. Mayoral[3], K. Kirov[3], J. Mailloux[3], S. Heuraux[4], E. Faudot[4], J. Ongena[5], ASDEX Upgrade team and JET EFDA contributors*

[1]Association Euratom - CEA pour la Fusion Contrôlée, CEA-DSM-DRFC
[2]MPI für Plasmaphysik, Boltzmannstr. 2, D-85748 Garching, Germany
[3]EURATOM-UKAEA Fusion Association, Culham Science Centre, OX14 3DB, Abingdon, OXON, UK
[4]LPMIA, UMR 7040 CNRS,BP 239 F-54506 Vandoeuvre cedex, France
[4]ERM-KMS, Association EURATOM-Belgian State, Brussels
** See annex of M.L. Watkins et al, "Overview of JET Results ",*
(Proc. 21st IAEA Fusion Energy Conference, Chengdu, China (2006)).

Preprint of Paper to be submitted for publication in Proceedings of the
34th EPS Conference on Plasma Physics,
(Warsaw, Poland 2nd - 6th July 2007)

ABSTRACT

Recent experimental characterization of Radio Frequency (RF) - induced Scrape-Off Layer (SOL) modifications in ASDEX-Upgrade (AUG), JET and Tore Supra (TS) is summarized. Geometrical aspects are emphasised: complex SOL patterns are evidenced by several indicators visualized in one or two dimensions transverse to magnetic field lines. Results are ascribed to inhomogeneous RF-induced SOL biasing around powered Ion Cyclotron Range of Frequencies (ICRF) antennas and associated $E \times B_0$ density convection [D'Ippolito1993]. Within a simple RF sheath model [9], the shape of convective cells on TS can be interpreted in terms of RF sheath generation by parallel RF currents. Some lessons are drawn for future machines.

1. INTRODUCTION

Since the first Ion Cyclotron Range of Frequencies (ICRF) heating systems in magnetic fusion devices, the non-linear physics of ICRF waves in the plasma edge has received considerable attention. In the prospect of ITER, the topic has recently gained renewed interest, with ICRF operation in all-metal machines (AUG, C-mod, future Be wall on JET), over long pulses (LHD, Tore Supra (TS)), or in combination with other subsystems, such as Lower Hybrid Current Drive (LHCD on TS, JET, C-mod).

Rather than an exhaustive review, already available in previous literature (e.g. [24]), the present paper summarizes recent experimental characterization of RF-induced SOL modifications on AUG, JET and TS. Complementary experiments are carried out in C-mod [32], [33], [31]. Emphasis is put on geometrical aspects. Resolving complex SOL patterns, in relation with the topology of RF currents over ICRF antenna front faces, puts severe constraints on interpretative physics models. Accurate LH launcher positioning in the highly inhomogeneous ICRF antenna environment is also essential to high power combined scenarios [13], [20]. Finally, geometry provides hints for front face design improvement, judicious port allocation, and which plasma facing components should be protected in future machines.

The paper is organized as follows. Indirect indications of inhomogeneous SOL changes are first presented: localized sputtering yield enhancement, asymmetric LH coupling modifications. LH heat fluxes are mapped in two dimensions (2D) transverse to magnetic field lines. More direct 2D characterization is performed on TS with a reciprocating probe combined with a scan of the edge safety factor

$q(a)$. The final section tries to synthesise the experimental results into a coherent picture, proposes elements of interpretation, and draws lessons for future machines.

2. LOCALIZED SPUTTERING YIELD ENHANCEMENT.

The fast magnetosonic wave used for ICRF heating is launched to the plasma from antennas located at the low field side of the vacuum vessel (e.g. inset of figure 3). Active elements form an array of poloidal radiating straps that can be phased toroidally to tailor the launched wave spectrum and

allow current drive. AUG and TS antennas include two straps, while JET A2 antennas have four. When not mentioned, antisymmetric strap phasing [0,π] was used, in D(H) minority heating scenario. In most recent antennas the straps are housed in individual boxes, partially closed on the plasma side by a tilted Faraday screen. Antennas are protected from plasma influx by side limiters.

Since 2006, 85% of plasma facing components in AUG are tungsten (W) coated, including ICRF antenna poloidal limiters. Dedicated spectroscopic observations monitor W erosion on several poloidal lines of sight, aiming either at an antenna limiter or a magnetically connected guard limiter [Dux2007]. In ICRF-heated discharges, the antenna limiter systematically exhibits both higher W fluxes and higher effective sputtering yields Y^{eff} than the guard limiter [11], [3]. Y^{eff} is an indicator of primary ion energy, whose increase was estimated between 1eV and 100eV. Sputtering is enhanced with [0,π/2] strap phasing, especially on high triangularity plasmas [3]. Comparison of poloidal lines of sight suggest higher Y^{eff} towards the top of the antenna than near the equatorial plane. The ratio Y^{eff}(antenna)/ Y^{eff}(guard) was used to quantify the degree of localization of RF-induced interaction with the plasma [4]. Figure 1 shows higher localization with higher ICRF power and smaller antenna-plasma distance. At the same time absolute W influx and Y^{eff} were higher. To reduce the W sputtering yield a low plasma temperature at the limiters was found preferable and was obtained at high density.

On C-mod, enhanced Mo erosion was observed not on powered ICRF antennas themselves but on field lines passing in front of them [32], [33]. Fe and Cu radiation was monitored during ICRF on TS [22]. Over a scan of H minority concentration a minimum was found in metallic impurity brightness, corresponding with good single pass absorption of the fast wave.

3. ASYMMETRIC LH COUPLING MODIFICATIONS.

LH waves are launched to the plasma by phased waveguide arrays, such as the TS grill C2 on the inset of figure 2. The power reflection coefficient C_{ref} of LH waveguide modules is sensitive to the local density n_{C2} measured by a fixed dome probe located in the equatorial plane on the grill. Figure 2.a) shows that C_{ref} is low at high density and progressively increases as n_{C2} drops below the cut-off density for the slow wave ($1.7\times10^{17}\mathrm{m}^{-3}$ at 3.7GHz).

Figure 2 summarizes LH coupling properties over a radial scan of grill C2 and for several combinations of the two ICRF antennas Q1 and Q5 surrounding the LH launcher. 1MW total ICRF power was applied, with different power splitting. Interaction with ICRH displaces the working point of lower LH modules towards the low density part of the characteristic curve on figure 2.a). The magnitude of density reduction depends on antenna combination and on grill radial position. The third TS ICRF antenna is not connected and does not influence C_{ref}. This tendency, first evidenced on JET and TS [13], is now also observed on C-mod [31]. Over the experiment C_{ref} on lower modules remains correlated with n_{C2} on probe 3, directly connected to the third waveguide row. Larger scatter appears with upper modules on figure 2.b), both towards LH coupling degradation or improvement, suggesting poloidal density imbalance.

C_{ref} was therefore mapped in 2D on figure 3 as a function of the connection point of LH modules

in a reference poloidal plane containing the septum of the powered ICRF antenna. Connection points are labelled by their altitude Z and their radial distance δr to ICRF antenna limiters (see inset). Due to field line pitch angle at $q(a)$=5.2, grill C2 explores the upper part of Q5 and the lower part of Q1 antenna, as featured by the two coloured areas. When the grill is 1cm behind antennas, LH coupling is initially difficult but improves on top modules with application of Q5 antenna. When antenna Q5 and grill C2 are combined, and as the grill is retracted away from the plasma, C_{ref} first increases and then drops on upper modules, suggesting a local density minimum over the radial scan. With other antenna combinations C_{ref} grows monotonically, and n_{C2} on probe 3 always decreases with increasing distance to the plasma.

Asymmetry is even more striking on the JET LH grill, whose 6 rows of waveguides offer more spatial resolution than on TS. LH coupling is modified only by ICRF antennas A and B, which are magnetically connected to the grill [20]. Antenna A is usually not connected to the upper part of the LH grill and therefore does not affect the coupling of the upper rows whilst C_{ref} on the bottom three rows are larger at higher P_{antA}. Degradation of the coupling with P_{antB} is generally observed and C_{ref} always increases with the distance between the launcher and the limiter. However, improvement also occurs, with opposite variations of C_{ref} on different rows over the same RF pulse. Poloidal as well as toroidal asymmetries were found, partly due to a mismatch of the plasma poloidal shape with the grill curvature. The coupling clearly depends on RF antenna phasing. Figure 4 shows that it is worse when antenna B is powered in –p/2 or monopole phasing, as compared to dipole and +p/2. Strong differences in C_{ref} behaviour suggest that the local electron density modifications are not poloidally symmetric. Gas puffing from a nearby gas injection module was shown to improve LH coupling in combined pulses: it compensates density depletion by local ionisation. This technique is now routinely used in experiments that require power from LHCD and ICRF antenna B [12], [20].

4. 2D MAPPING OF LH HEAT FLUXES ON TORE SUPRA

Electron acceleration in the LH parallel near field produces localized heat loads on field lines passing in front of each waveguide row [16], [28]. For a given LH launcher geometry and fixed $n_{//}$, the parallel heat flux $Q_{//}$ increases with the local density and with the LH near field magnitude [15], [16]. This magnitude is determined by the launched power and by C_{ref} (i.e. n_e again). In thermal steady-state, the surface temperature elevation ΔT_{IR} on the actively cooled side limiters of grill C2 is proportional to $Q_{//}$. ΔT_{IR} is monitored by infrared cameras [18], and feeds a real-time safety system [23] to prevent over-heating in high power scenarios [13].

Figure 5 shows typical time evolutions of ΔT_{IR} over a combined ICRH+LHCD pulse. In ohmic phase the left side limiter of grill C2 remains cool. As grill C2 is powered alone, a hot spot appears in front of each waveguide row. All four zones reach similar steady-state temperatures in typically 7s. When antenna Q5 is added, ΔT_{IR} evolution becomes poloidally asymmetric. At the same time, LH coupling shows opposite evolution and density drops promptly on probe 3, connected to row 3. For given plasma density, ICRF and LH powers, the final value of ΔT_{IR} depends on the waveguide

row, on which ICRF antenna Q1 or Q5 is operated, and on the relative radial positions of ICRH and LH launchers.

Steady-state ΔT_{IR} was therefore mapped in 2D for the same series of RF pulses as on figure 3. Figure 6.a) obtained with grill C2 powered alone, shows moderate ΔT_{IR} with limited radial and poloidal variations. On figure 6.b), depending on magnetic connections, both temperature elevation and reduction are measured over the same combined RF pulse, resulting in large poloidal and radial gradients (up to 500^{o}C/cm). Strangely, when antenna Q5 is powered, the highest heat fluxes on the upper waveguide row are obtained with the grill retracted far away from the main plasma. This counter-intuitive behaviour is correlated with non-monotonous radial variations of C_{ref} on upper modules. However there is not always direct correspondence between C_{ref} and ΔT_{IR}, partly because C_{ref} mixes two waveguide rows. Lowest ΔT_{IR} are obtained with similar grill and antenna radial positions, on waveguide rows connected magnetically to the upper and lower parts of the antenna box.

5. 2D SOL CHARACTERIZATION.

More direct SOL characterization during ICRF was performed by various techniques in the past [1], [30], [19], [25], [2]. The observed SOL changes were generally interpreted in terms of profile modifications, whereas poloidal inhomogeneity also arises. SOL modifications were therefore mapped in 2D on TS by means of a reciprocating Langmuir probe, combined with $q(a)$ scans through plasma current steps [7]. When the ICRF antenna connected to the probe is powered, localised high positive peaks appear on the floating potential V_{float}. Similar biasing was evidenced in front of LH launchers [34]. The

ICRF-perturbed zone is radially centered near δr=0, with a radial width of typically 1cm on the connected side. V_{float} exhibits strong poloidal variation that is nearly symmetric with respect to the equatorial plane: a local minimum is observed near Z=0, and local maxima near lower and upper parts of the antenna box. The special role of TS antenna box corners was already pointed out in [29]. At given (dr,Z) position, small increase of V_{float} was found with local ICRF power (less than $P_{ICRF}^{1/2}$), and large decrease with plasma density [17].

Figure 7 shows that in the *perturbed zone*, the radial variation of the ion saturation current J_{sat} also strongly depends on Z. Near the equatorial plane J_{sat} keeps its value without RF power, or even increases. Local minima of J_{sat} were measured near top and bottom of the antenna box. They were centred near δr=0, with a typical radial extension 1cm on each side. This coincides with the low temperature zones of figure 6.b). The radial variations of J_{sat} are also consistent with non-monotonic behaviour of ΔT_{IR} and C_{ref}.

6. SYNTHESIS AND OUTLOOK.

Both sputtering and probe measurements suggest positive DC biasing of the ICRF antenna local environment. Several theoretical models predict RF-enhanced sheath potentials [26], [5], [21], [27],

[14], [10]. Within the simplest model [26], the relevant quantity for driving the sheaths is'$E_{//}$ integrated along open magnetic field lines. In [0,π] strap phasing, this integral was found maximal on long field lines passing in front of the upper and lower parts of the TS [8] and AUG [4] antenna box. Note however that some measurements were performed not *in front* but *behind* antenna side limiters. The radial width of the perturbed zone on figure 7 is of the order of the skin depth c/ω_{pe} for slow waves at $k_{//}$=0 (8mm for n_e=4.5×10^{17}m^{-3}). Slow wave excitation was attributed to parallel RF currents flowing in the box frame [6] and nearby Faraday screen rods [8]. As first proposed by [9], $\mathbf{E\times B_0}$ drift in the gradient of inhomogeneous V_{float} map produces convective cells, with $\mathbf{v_{E\times B}}$ directed upwards on the plasma side of the cells on TS and JET. A typical value of $v_{E\times B}$~3.5km/s was inferred from TS measurements [7]. This produces a complicated density pattern [2]: depletion is expected at the centre of the convective cells, while over-density is brought to the top of the antenna and behind the cells. Convection was already suspected on TS from a flip of asymmetric hot spot patterns upon magnetic field reversal [17]. The only way to reconstruct the pattern is 2D (perhaps 3D) mapping. On TS with [0,π] strap phasing, this picture seems consistent with observations both on the LH grill C2 and on the reciprocating probe. It is worth repeating the same exercise with other antenna geometries or strap phasings, in order to fully correlate the topology of sheath potentials with RF currents paths over different antenna front faces.

Some lessons can already be drawn for ITER. If the simple model in [26] reveals valid, future designs should reduce parallel RF currents on the antenna front face as well as on nearby metallic components (port, wall) in order to decrease sputtering during ICRF and improve compatibility with high-Z materials of the first wall. Furthermore high-Z materials should be used with care in antenna vicinity. LH-ICRF interaction can be easily reduced if magnetic connections are minimised by clever port allocation. Besides, gas injection helps increasing the local density on LH grills. The exact amount of gas should be determined from a trade-off between reliable LH coupling and reasonable heat fluxes from accelerated electrons, and should be applied at the place where density is depleted.

REFERENCES

[1]. Artemenkov L.I., Vukolov K. Yu., Gott Yu. V., et al., Proc. 15th EPS Conference on Controlled Fusion and Plasma Heating, Dubrovnik, May-1988, V 12B(II), 702

[2]. M. Bécoulet & al. *Phys. Plasmas*, **Vol. 9**, No. 6, p. 2619-2632, 2002

[3]. V.V. Bobkov et al., *Journal of Nuclear Materials* **363–365** (2007) 122–126

[4]. V.V. Bobkov et al., proc. 17th topical conf. on RF power in plasmas, Clearwater (Fa) 2007

[5]. M.D. Carter, et al. *Phys. Fluids* **B4** (5) may1992, p.1081

[6]. L. Colas, S. Heuraux, S. Brémond, G. Bosia, *Nucl. Fusion* **45** (2005) p.767–782

[7]. L. Colas et al., *Journal of Nuclear Materials* **363–365** (2007) 555–559

[8]. L. Colas & S. Heuraux, proc. 17th topical conf. on RF power in plasmas, Clearwater (Fa) 2007

[9]. D.A. D'Ippolito, J.R. Myra et al. *Phys. Fluids* **B5** (10), 1993, p. 3603

[10]. D.A. D'Ippolito, J.R. Myra,'*Physics of Plasmas* **13** 102508 (2006)
[11]. R. Dux et al., *Journal of Nuclear Materials* **363–365** (2007) pp. 112–116
[12]. A. Ekedahl & al., Proc. 15th Topical conf. On RF Power in Plasmas, Moran (Wy) 2003, AIP Conference Proceedings 694, pp. 259-262.
[13]. A. Ekedahl & al., proc. 17th topical conf. on RF power in plasmas, Clearwater (Fa) 2007
[14]. E. Faudot, S.Heuraux et al., *Physics of Plasmas* **13** 042512 (2006)
[15]. V. Fuchs, M. Goniche, Y. Demers, P. Jacquet, and J. Mailloux, *Phys. Plasmas* **3** (11), November 1996, pp. 4023-4035
[16]. M. Goniche & Al. *Nuclear Fusion* **38** (6) 1998, p. 919
[17]. M. Goniche et al. Proc. IAEA conf. Chengdu 2006
[18]. D. Guilhem et al., *Fusion Engineering and Design* **74,** 879 (2005)
[19]. Hanson G. R. et al. Proc. 11th Topical RF Conf., Palm Springs, 1995, p. 463.
[20]. K. Kirov et al., proc. 17th topical conf. on RF power in plasmas, Clearwater (Fa) 2007
[21]. M.A. Lieberman, V.A. Godyak, *IEEE trans. Plasma science* **26** 1998, p.955
[22]. O. Meyer et al., these proceedings.
[23]. Ph. Moreau & al., proc. SOFT 2006 Varsaw, *Fusion Engineering and Design* doi:10.1016/ j.fusengdes.2007.01.022.
[24]. Noterdaeme J.-M. and Van Oost G. *Plasma Phys.Control. Fusion* **35** (1993) p. 1481 and references therein.
[25]. Noterdaeme J.-M., et al., 23th EPS Conf. Plasma Phys., Kiev, 1997. p. 723
[26]. Perkins F., *Nucl. Fusion* **29** 4 (1989), 583
[27]. V. Petr~ilka & al., 22nd EPS conf. Plasma Phys. 2005, ECA Vol.**29C**, P-2.095
[28]. V. Petr~ilka et al., proc. 33rd EPS Conference on Plasma Phys. Rome, 19 - 23 June 2006 ECA Vol.**30I**, P-5.108 (2006)
[29]. Thomas C. E., Harris J. H., et al, *Fusion Technology* **30** (1996), 1.
[30]. G. Van Oost, et al. *Fusion Eng. Design* **12** (1990), p. 149
[31]. G. Wallace et al., proc. 17th topical conf. on RF power in plasmas, Clearwater (Fa) 2007
[32]. S. Wukitch et al., *Journal of Nuclear Materials* **363–365** (2007) 491–497
[33]. S. Wukitch et al., proc. 17th topical conf. on RF power in plasmas, Clearwater (Fa) 2007
[34]. F. Zacek, V. Petr~ilka, M. Goniche, *PPCF* **47** 2005 n°7 L17

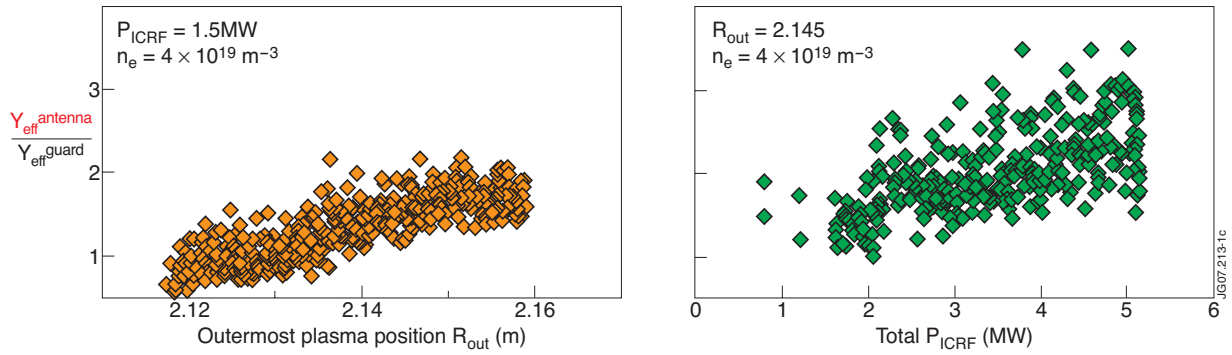

Figure 1: Degree of localization of RF-induced W sputtering on AUG. a) Dependence on outermost plasma position. b) Dependence on RF power. Adapted from [4]

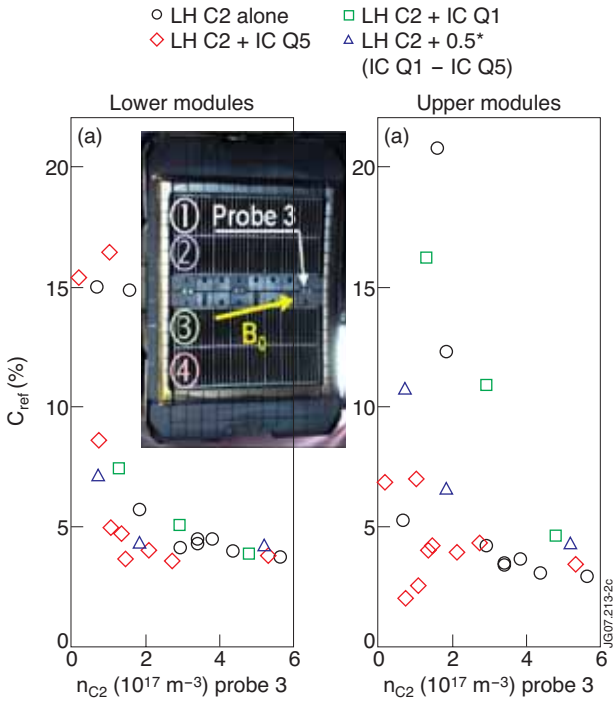

Figure 2: LH power reflection coefficient C_{ref} vs local density n_{C2} measured by probe 3 on the equatorial plane of grill C2 (Tore Supra). Measurements obtained over a radial scan of grill C2, for different combinations of neighbouring ICRF antennas Q1 and Q5. Left: average over lower LH modules; Right: average over upper modules. Inset: photograph of grill C2, with location of probe 3, sketch of magnetic field line pitch and waveguide row numbering for figure 5.

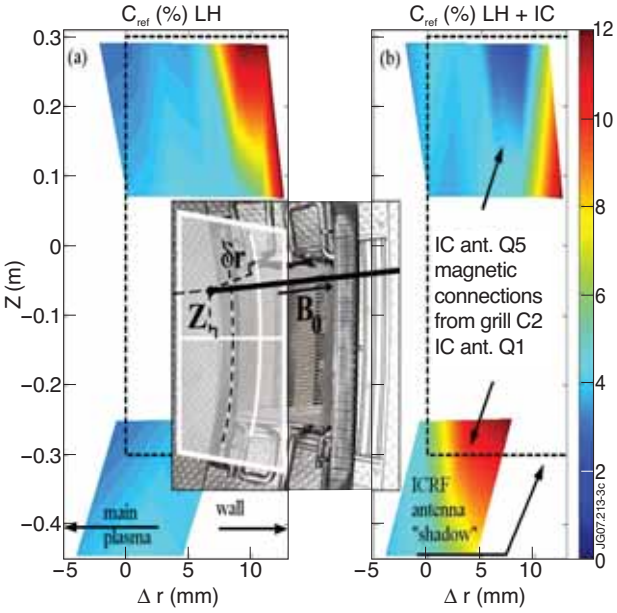

Figure 3: Color map of LH power reflection coefficient on TS grill C2, for the set of RF pulses in figure 1. Left with grill C2 powered alone (1MW) ; Right grill C2 (1MW) combined with connected ICRF antenna (either Q1 or Q5, 1MW). Same color scale on two panels. Vertical dashed line: leading edge of ICRF side limiter; horizontal dashed lines: vertical extension of ICRF antenna box. Inset: photograph of TS ICRF antenna, and sketch of the 2D coordinate system used for mapping.

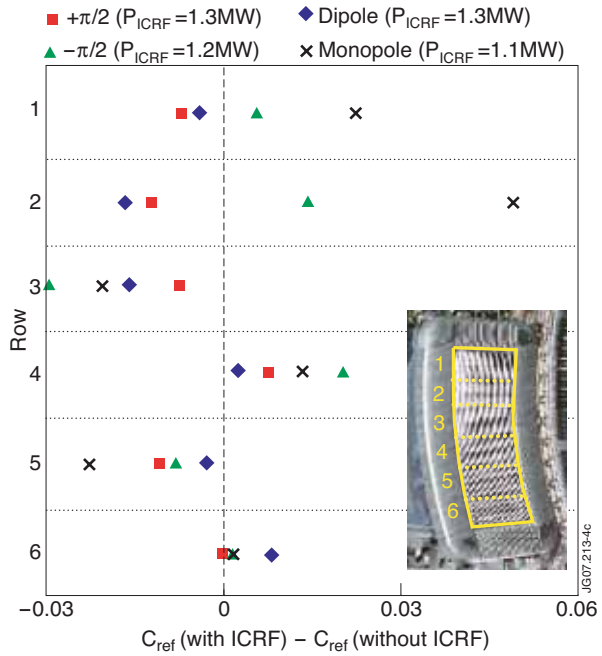

Figure 4: Variation of reflection coefficient during ICRF, averaged over each row of the JET grill, in combined pulses with ICRF antennas A and B, and for four strap phasings. Plasma parameters: magnetic field 2.6T; plasma current 1.5MA; L-mode; LH launcher position 2.5cm behind limiters; 7◊10^{21}e^{-}/s D_2 puffed from near gas pipe. Inset: photograph of JET LH launcher with row numbering from top to bottom.

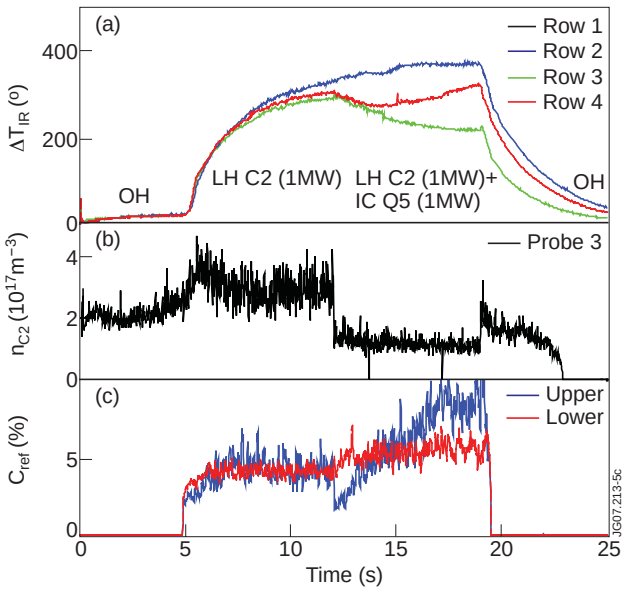

Figure 5. Grill C2 time behavior during combined LHCD+ICRF pulse TS 38071. a) Surface temperature elevation on left side limiter, in front of each waveguide row (Row numbering: see figure 2); b) local density measured by probe 3 (connected to row 3); c) power reflection coefficient averaged over upper and lower LH modules.

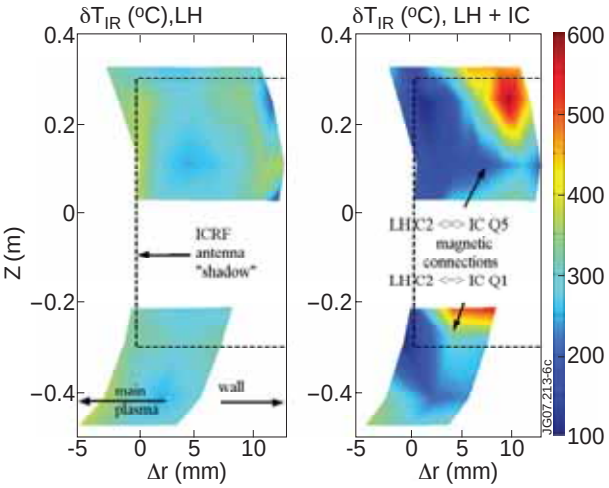

Figure 6: 2D mapping of steady-state temperature elevation on left side limiter of grill C2, in the same coordinate system as on figure 3. a) with grill C2 powered alone (1MW); b) grill C2 (1MW) combined with connected ICRF antenna (either Q1 or Q5, 1MW). Same color scale on the two panels.

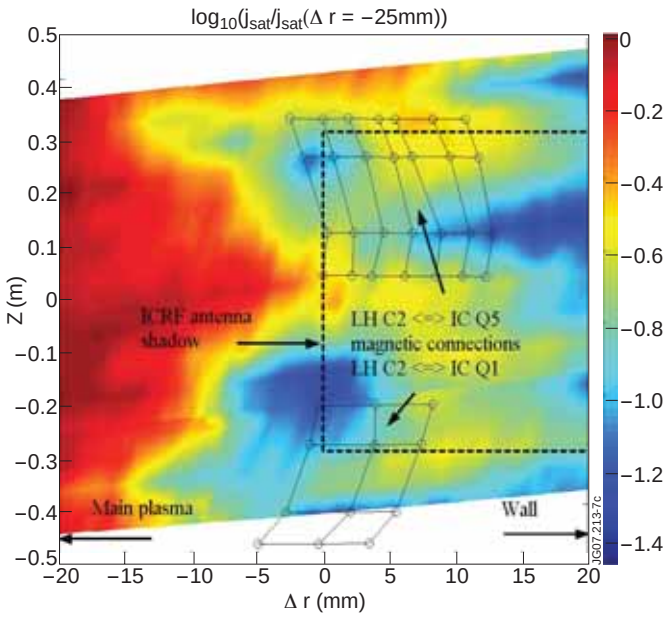

Figure 7: 2D mapping of ion saturation current measured by reciprocating Langmuir probe, in the same coordinate system as on figure 3. The current is normalized to its value in dr=-25mm and plotted in logarithmic scale. Measurements were made with the probe connected to powered antenna Q5 (1.5MW). Superimposed: magnetic connections from grill C2 to the two neighboring ICRF antennas Q1 and Q5 on figure 3 and 6.